



Design of F-Shaped Slot Triple Band Antenna for WLAN/WiMax Applications

Visvesvaran¹ Induja² Sumathy³ Tamilarasi⁴
Department of ECE, Sri Krishna College of Engineering and Technology,
Coimbatore, Tamil Nadu, India

Abstract—This communication presents a small, low-profile planar triple-band microstrip antenna for WLAN/WiMAX applications. The goal of this communication is to combine WLAN and WiMAX communication standards simultaneously into a single device by designing a single antenna that can excite triple-band operation. The designed antenna has a compact size of $19 \times 25 \text{ mm}^2$ ($0.152 \lambda_0 \times 0.2\lambda_0$). The proposed antenna consists of F-shaped slot radiators and a defected ground plane. Since only two F-shaped slots are etched on either sides of the radiator for triple-band operation, the radiator is very compact in size and simple in structure. The antenna shows three distinct bands I from 2.0 to 2.76, II from 3.04 to 4.0, and III from 5.2 to 6.0 GHz, which covers entire WLAN (2.4/5.2/5.8 GHz) and WiMAX (2.5/3.5/5.5) bands. To validate the proposed design, an experimental prototype has been fabricated and tested. Thus, the simulation results along with the measurements show that the antenna can simultaneously operate over WLAN (2.4/5.2/5.8 GHz) and WiMAX (2.5/3.5/5.5 GHz) frequency bands.

Index Terms—Multiband antenna, triple band, WiMAX, WLAN application.

I. INTRODUCTION

Mobile devices, such as hand-held computers and smart phones, are widely using wireless local area network (WLAN) and worldwide interoperability for microwave access (WiMAX) for Internet access. The WLAN/WiMAX module, used to avail of these environments, is capable of operating at multiple frequency bands. Due to the appealing features, such as simple feeding, low profile, low manufacturing cost, and easy-to-integrate, the microstrip patch antennas are the most popular candidates for these devices. The federal communication commission (FCC)-specified spectrum for WLAN is centered at 2.4, 5.2, and 5.8 GHz and for WiMAX at 2.5, 3.5, and 5.5 GHz. However, a number of microstrip antennas with different geometries have been experimentally characterized to reduce the size and enhance the bandwidth for WLAN/WiMAX applications [1]–[9]. A square slot, a pair of L-strips, and a monopole radiator are used to excite three different resonances in [1]. In [2], a microstrip feed line, a substrate, and a ground plane on which some simple slots are etched to achieve triband operation. A nonuniform meander-line and a fork-type ground are proposed for triple-band WLAN applications in [3]. An asymmetric M-shaped patch is used to design a triple-band antenna, and vias on the longer arm of the patch are used for the purpose of compactness [4]. Inverted L-slot patch with a defected ground plane is used for triple-band operation, whereas three circular-arc-shaped strips whose whole geometry looks like “ear”-type antenna are reported to cover the desirable bands for WLAN/WiMAX wireless

communication terminal in [6]. An F-shaped microstrip slot antenna with both open-ended and short-ended slots connected by a metal “via” to a microstrip line is exploited for WLAN and WiMAX multiple-input multiple-output (MIMO) systems in [7]. A monopole antenna with two rectangular corners cut off and two inverted-L slots

TABLE I
PERFORMANCE COMPARISON OF THE PROPOSED ANTENNA WITH OTHER REPORTED ANTENNAS

Ref.	Size (mm×mm)	Operating bands (GHz)
		WLAN (2.4-2.5 GHz, 5.2-5.8 GHz) WiMAX (2.3-2.6 GHz, 3.3-3.8 GHz, 5.7-5.85 GHz)
[1]	28 × 32	2.34–2.8, 3.16–4.06, 4.69–5.37
[2]	35 × 30	2.4–3.0, 3.25–3.68, 4.9–6.2
[3]	120 × 40	2.39–2.90, 4.97–5.98
[4]	64 × 62	2.38–2.49, 3.49–3.63, 5.57–6.20
[5]	20 × 30	2.39–2.51, 3.15–3.91, 4.91–6.08
[6]	18 × 37	2.35–2.53, 3.34–3.85, 5.05–6.28
[7]	18 × 37	2.38–2.78, 3.28–3.76, 4.96–5.96
[8]	33 × 36	2.28–2.66, 3.35–3.65, 5–5.3, 5.73–5.85
[9]	50 × 90	2.4–2.484, 5.15–5.35, 5.7–5.82
[10]	21 × 29	2.39–2.51, 3.38–3.72, 4.79–6.24
[11]	23 × 36.5	2.33–2.76, 3.05–3.88, 5.57–5.88
[12]	23 × 36.5	2.0–2.15, 2.75–3.52, 5.4–5.9
[13]	11 × 33	2.3–2.7, 3.3–3.8, 4.9–5.85
[14]	40 × 45	2.3–4, 5–6.6
Proposed	19 × 25	2.0–2.76, 3.04–4.0, 5.2–6.0

are etched to achieve three resonant modes for triband operation is presented in [8]. An asymmetric coplanar strip (ACS)-fed structure was introduced in [9], MTM-inspired reactive loading, and metamaterial transmission lines are used in [10] and [11], respectively, for triple-band operation. In [12], a frequency-agile triple-band microstrip antenna using defected ground structure is presented, and in [13], a meandering splitting slot is proposed to generate three distinct bands. In [14], the antenna can cover the required bands with an extremely small form factor with the aid of the MTM-inspired reactive loading and L-shaped slot. Although, all the reported antennas exhibit triple-band performance, but in comparison, the proposed antenna occupies the smallest area and has simpler geometry to realize the required operating bands compared to other designs as shown in Table I.

In this communication, a compact F-shaped planar antenna is proposed and designed for wireless communication systems that can support the triple-band WLAN/WiMAX applications. The proposed antenna consists of two F-shaped slots of the same size that are etched on a rectangular patch to achieve multiband operation. The impedance matching in this design is achieved by printing a circular shape patch that is gap-coupled with rectangular ground plane on the other side of dielectric substrate. The proposed antenna shows three distinct resonances with impedance bandwidths of 2.0–2.76 GHz (760 MHz), 3.04–4.0 (964 MHz), and 5.2–6.0 GHz (800 MHz), respectively. The antenna configuration has a compact size of 19 mm × 25 mm. Since the F-shaped slots are etched on the left and right sides of the radiator for triple-band operation, the antenna is very compact in size and simple in structure. To validate the proposed design, an experimental prototype has been fabricated and

II. ANTENNA CONFIGURATION AND DESIGN APPROACH

Fig. 1 shows the geometry and dimensions of the proposed triple-band antenna for WLAN and WiMAX triple-band operation. The proposed antenna is fabricated on the FR4 dielectric substrate of thickness 1.6 mm, relative permittivity of 4.4, and dielectric loss tangent of 0.02. The overall size of the proposed antenna is only 19 mm × 25 mm or about $0.152\lambda_0 \times 0.2\lambda_0$, where λ is the free-space wavelength at the desired first resonant frequency 2.4 GHz. The antenna is composed of a rectangular-shaped radiator with two F-shaped slots of equal size, formed by dimensions W_1 , L_1 , W_2 , and L_2 , which are etched on the left and right side of the radiator. A circular-shaped patch is printed with a rectangular ground plane on the backside of the dielectric substrate. Christo Ananth et al. [5] discussed about E-plane and H-plane patterns which forms the basis of Microwave Engineering principles.

Computer simulation technology (CST), microwave studio (MWS), and Ansoft's HFSS commercial software are used to optimize parameters for triple-band operation of the proposed compact antenna, and the dimensions are listed in Table II.

The antenna design evolution process to achieve the triple-band operation for WLAN/WiMAX applications is shown in Fig. 2. The antenna design starts by a conventional rectangular patch and ground plane, and from Fig. 3, it can be observed that in this case a single resonant mode seems to form at about 3.0 GHz (see Ant 1). The Ant 2 (Fig. 2) shows that two modes are resonating at 2.8 and 4.2 GHz due to the modification of the radiating patch by etching two L-shaped slot each on either boundaries of the patch. Ant 3 indicates that inclusion of an additional L-shaped slot on the radiating

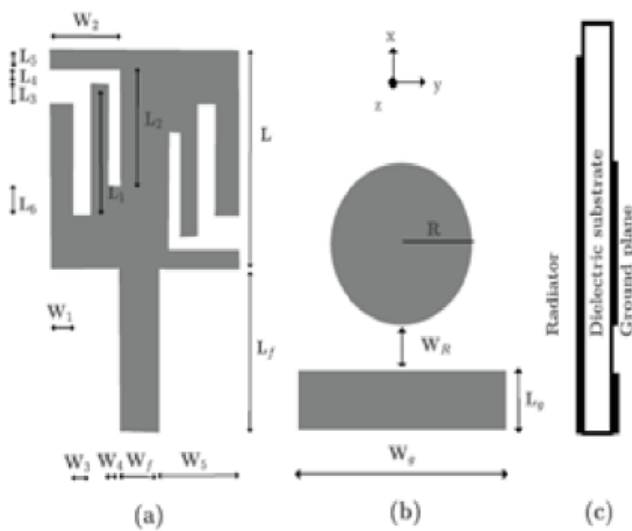


Fig. 1. Schematic configuration of the proposed triple-band antenna. (a) Top view. (b) Bottom view. (c) Side view.

TABLE II
DESIGN PARAMETERS OF THE PROPOSED ANTENNA

Parameters	Unit (mm)	Parameters	Unit (mm)
L	15.0	W_R	2.8
L_1	9.0	W_1	1.25
L_2	8.8	W_2	5.25
L_3	0.6	W_3	1.0
L_4	1.0	W_4	0.4
L_5	1.0	W_5	6.25
L_6	1.2	R	7.9
L_g	3.9	W_g	19.0
L_f	9.0	W_f	3.0

tested. Details of antenna design and the simulated and measured results are presented and discussed in the following sections.

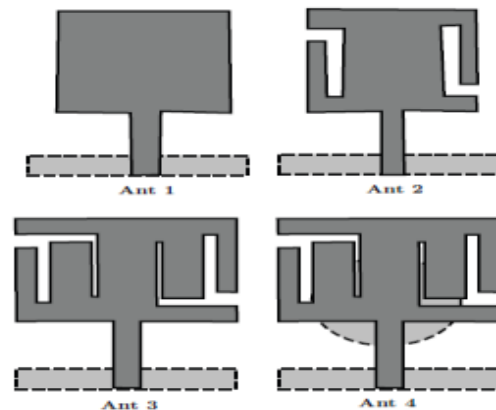


Fig. 2. Antenna geometry evolution for the proposed design.

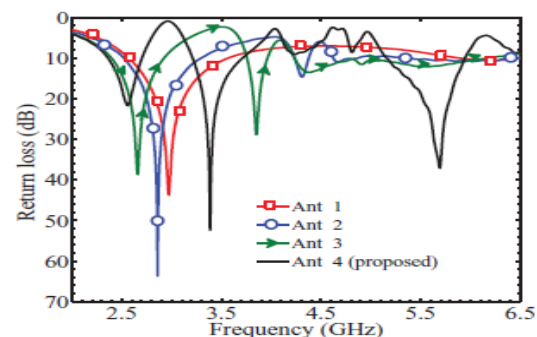


Fig. 3. Simulated return loss against frequency for the various antenna configurations.

patch of the antenna provides another additional resonance. Finally, ground plane is modified by printing circular-shaped patch to improve the impedance matching (Fig. 3).

To study the operating principle and the relationship between resonant frequencies and important parameters of the antenna, the simulated surface current distributions are plotted at the sample frequencies of 2.55, 3.39, and 5.69 GHz, which are shown in Fig. 4. From Fig. 4(a), one can find that the strong surface current concentrates on the main radiating patch and on the right side of the F-slot patch. Therefore, it can be understood that the 2.4-/2.5-GHz WLAN resonance occurs due to the middle and right side of the patch. For the 3.5-GHz operation [see Fig. 4(b)], it is observed that the resonance occurs due to F-shaped slot on the left-hand side of the patch. The third (highest) resonant mode of the antenna, by considering the current distribution of the antenna as shown in Fig. 4(c), arises from the currents on the upper and lower strip formed due to the F-shaped slots on the radiating patch and feed line. This clearly indicates the importance of the embedded slot on the proposed antenna resonance. Moreover, at this frequency, a strong current distribution is noticed on the finite ground plane around the circular strip. Further analysis shows that the circular strip on the ground plane improves the impedance matching and the bandwidth of the mode; it does not contribute to the third resonance. Thus, from the current distribution, it can

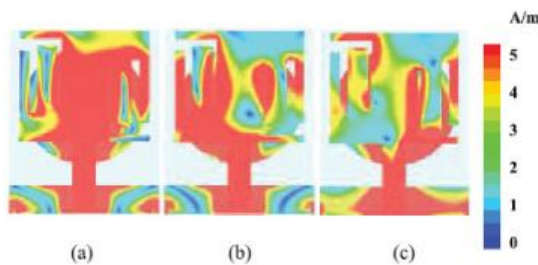


Fig. 4. Simulated surface current distributions at (a) 2.55 GHz, (b) 3.5 GHz, and (c) 5.69 GHz.

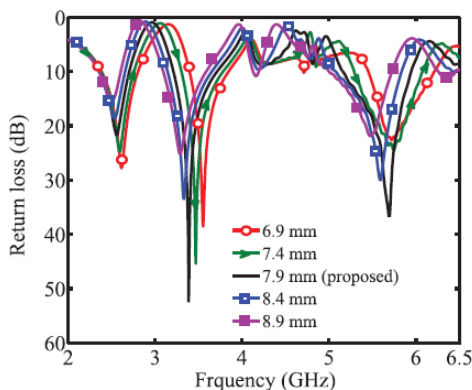


Fig. 5. Simulated return loss against frequency for the proposed antenna with various R; other parameters are the same as listed in Table II.

be concluded that the proposed antenna can generate triple band covering the 2.4-/5.2-/5.8-GHz WLAN and 2.5-/3.5-/5.5-GHz WiMAX bands. Fig. 5 shows the effect of radius R of the circular patch beneath the radiator and gap-coupled with ground plane on return loss of the antenna. Results show that the radius R influences

the antenna performance significantly. By increasing the radius to 7.9 mm, all modes are excited, and bandwidth and impedance matching are improved considerably. Further increasing the radius from 7.9 to 8.9 mm, all the frequency bands shift toward the lower frequency. According to this, the optimal value of radius (R) of the circular patch beneath the radiator is chosen as 7.9 mm. The design strategy for the excitation of triple band and to calculate the first-cut dimensions of the L-shaped patch and the slots has been explained as follows.

A. First Resonance

The first resonance in the proposed antenna is excited due to the middle and right side of the patch. At the resonance, this length would be half of the wavelength in the medium. The boundary condition for the first resonance can be seen from Fig. 4(a), in which the maxima of the current occur at the main radiating patch and the right-side F-slot patch; therefore, the length of the radiating patch responsible for first resonance can be calculated as

$$L_{r1} = (L - L_5) + (W_f + W_5) + (L_2 + L_6 - L_4). \quad (1)$$

From the data presented in Table II, $L_{r1} = 32.25$ mm. Here, the effective dielectric constant of the antenna is calculated based on the equation given in [15]. Therefore, the effective dielectric constant (ϵ_{eff}), due to the circular patch beneath the radiating patch, is 3.86.

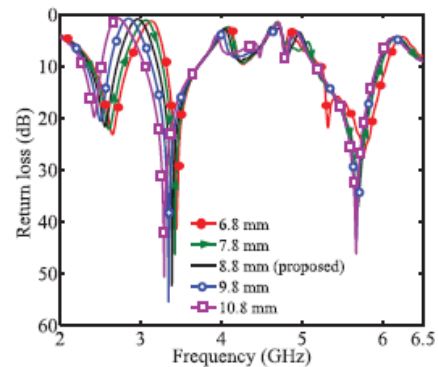


Fig. 6. Simulated return loss against frequency for the proposed antenna with various L_2 of F-slot on the right-hand side of the radiating patch; other parameters are same as listed in Table II.

TABLE III
COMPARISON BETWEEN DESIGN EQUATION AND FULL WAVE SIMULATION FOR FIRST RESONANCE

L_2 (mm)	L_{r1} (mm)	Resonant frequency (GHz)		% difference
		Design equation	Full-wave simulation	
6.8	30.25	2.53	2.64	4.16
7.8	31.25	2.45	2.61	6.13
8.8	32.25	2.37	2.55	7.01
9.8	33.25	2.3	2.50	8.0
10.8	34.25	2.23	2.42	7.8

At the resonance, L_{r1} should be $\lambda_g/2$. Therefore,



$$f_{r1} = \frac{c}{2L_{r1}\sqrt{\epsilon_{reff}}} \approx 2.37 \text{ GHz.}$$

The effectiveness of the design method is further validated by predicting the first resonance frequency for the data presented in Fig. 6. In Table III, the first resonant frequency as a function of L_2 is compared with the full-wave simulated data. Fig. 6 clarifies the effect of L_2 of the F-shaped slot on the right-hand side of the radiator on return loss of the antenna. As seen in Fig. 6, by varying the slot length L_2 , there is no significant change in the second and third resonance, whereas the first resonance is very sensitive to this dimension. As the length is increased from 6.8 to 10.8 mm, the first resonance shifts toward lower frequency side. Further increase in length spoils the boundary condition necessary for the first resonance. Hence, to cover the triple-band accurately, the value of L_2 is selected to be 8.8 mm. From Table III, it can be seen that the resonant frequencies calculated from the design method are agreeing well with the simulated data.

B. Second Resonance

The second resonance is excited due to the F-slot on the left-hand side of the radiating patch, which is evident from Fig. 7. However, for the boundary condition in this case, the electric field maxima occur at the slot edges as shown in Fig. 4(b). From the data given in Table II, the length of the slot is 23.05 mm, as

$$L_2 = L_1 + L_2 + W_2. \quad (3)$$

Therefore, $f_2 = 3.31$ GHz for $\epsilon_{reff} = 3.86$. However, the full-wave Simulations shows that the resonance is occurred at 3.43GHz, which

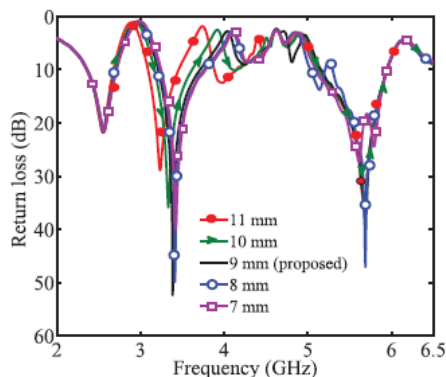


Fig. 7. Simulated return loss against frequency for the triple-band antenna with various L_1 of the F-slot on the left-hand side of the radiating patch; other parameters are same as listed in Table II.

TABLE IV
COMPARISON BETWEEN DESIGN EQUATION AND FULL WAVE SIMULATION FOR SECOND RESONANCE

L_1 (mm)	L_{r2} (mm)	Resonant frequency (GHz)		% difference
		Design equation	Full-wave simulation	
7	21.05	3.62	3.5	3.3
8	22.05	3.46	3.43	0.8
9	23.05	3.31	3.39	2.3
10	24.05	3.27	3.34	2.1
11	25.05	3.10	3.23	4.0

is much close to the predicted value. The effectiveness of the design method is further validated by predicting the second resonance frequency for the data presented in Fig. 7. In Table IV, the second resonant frequency as a function of L_1 is compared with the full-wave simulated data. From Fig. 7 and Table IV, it can be seen that the resonant frequencies calculated from the design method are agreeing well with the simulated data.

C. Third Resonance

The third resonance occurs due to the narrow strips, formed due to the F-shaped slot at the bottom and right-hand side on the radiating patch, respectively. This can also be established by studying the current distribution as shown in Fig. 4(c). In this figure, it is clearly shown that one of the current minima occurs at the end of the edge and the other on the feed line. At resonant frequency, the length of the current path would be half of the guided wavelength. Therefore,

$$L_3 = L_2 + W_2 - W_4. \quad (4)$$

Here, the effective dielectric constant of the medium is 3.86. The effectiveness of the design method is further validated by predicting the third resonance frequency for the data presented in Fig. 8. In Table V, the third resonant frequency as a function of W_2 of the right side is compared with the full-wave simulated data.

From Fig. 8 and Table V, it can be seen that the resonant frequencies calculated from the design method are agreeing well with the simulated data.

III. EXPERIMENTAL RESULTS AND DISCUSSION

After optimization, the proposed antenna was fabricated with the MITS-Eleven Lab PCB machine. Then, to validate the simulation

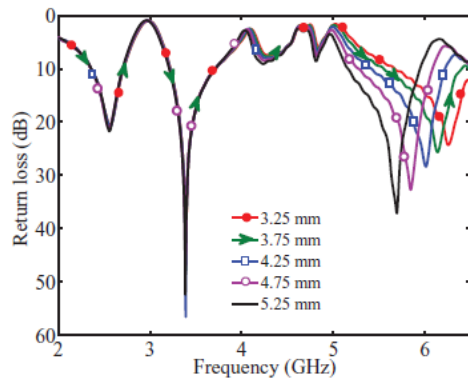


Fig. 8. Simulated return loss against frequency for the triple-band antenna various W_2 of the F-slot on the right-hand side of the radiating patch parameters are same as listed in Table II.

TABLE V
COMPARISON BETWEEN DESIGN EQUATION AND FULL WAVE SIMULATION FOR THIRD RESONANCE

W_2 (mm)	L_{r3} (mm)	Resonant frequency (GHz)		% difference
		Design equation	Full-wave simulation	
5.25	13.65	5.59	5.69	1.75
4.75	13.15	5.8	5.85	0.8
4.25	12.65	6.04	6.00	0.66
3.75	12.15	6.28	6.15	2.1
3.25	11.65	6.55	6.26	4.42

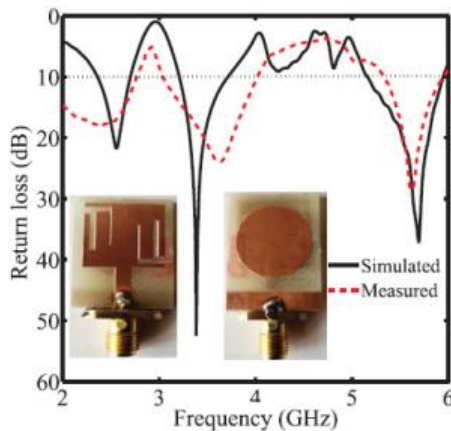


Fig. 9. Measured and simulated results of return loss for the proposed compact slot antenna.

results, the antenna parameters were measured by an Agilent N5230A vector network analyser. The return loss was measured and the obtained result together with the simulated one are shown in Fig. 9. It can be observed that the simulated and measured results display a good agreement. The differences between the measured and simulated results are probably due to the fabrication tolerance, substrate losses, and measurement circumstances. According to the measured results, it is found that the proposed compact antenna can effectively cover three separate impedance bandwidths of 760 MHz (2.0–2.76 GHz), 996 MHz (3.04–4.0 GHz), and 800 MHz (5.2–6.0

GHz), which can well satisfy both the 2.4-/5.2-/5.8-GHz WLAN bands and 2.5-/3.5-/ 5.5-GHz WiMAX bands.

Gain and efficiency variation with the frequency is shown in Fig. 10. It is found that the gain remains consistent throughout all the three

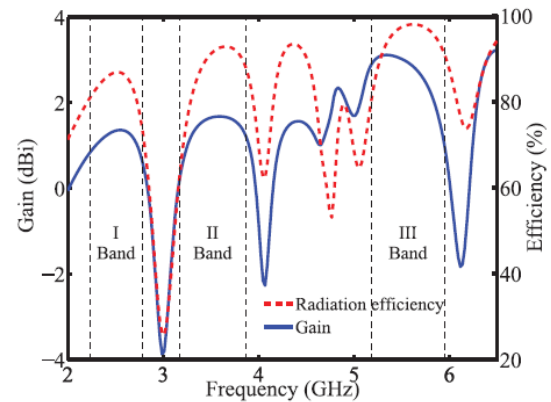


Fig. 10. Gain and efficiency of the proposed compact triple-band antenna.

TABLE VI
THE GAIN AND EFFICIENCY AT THE CENTER FREQUENCIES OF WLAN/WiMAX BANDS

Parameters	2.5 GHz	3.5 GHz	5.5 GHz
Gain (dBi)	1.5	1.7	3.05
Efficiency (%)	87	92	95

bands and it varies from 1.48 to 1.78 dB in I band, from 1.438 to 1.84 dB in II band, and from 1.6 to 3.1 dB in III band. It is also observed from Fig. 10 that the radiation efficiency of the antenna varies from 70 to 95%. Both the gain and efficiency drop drastically for frequencies other than the resonant bands. Table VI lists the gain and efficiency at the center frequencies of WLAN/WiMAX bands.

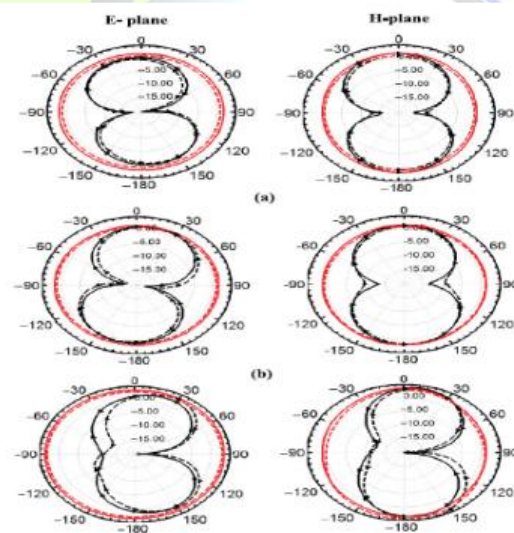


Fig. 11. Measured and simulated radiation patterns of the proposed antenna. (a) 2.5-GHz, (b) 3.5-GHz, and (c) 5.5-GHz resonance frequencies. H-field (xy-plane) and E-field (xz-plane).



International Journal of Advanced Research Trends in Engineering and Technology (IJARTET)
Vol. 4, Special Issue 7, March 2017

The radiation characteristics of the proposed design are also studied,

and for brevity, the radiation patterns are given at the central operating frequency in each band. Fig. 11(a)–(c) shows the two-dimensional (2-D) far-field radiation patterns in the H- and E-planes at sampling frequencies of 2.5 GHz, 3.5 GHz, and 5.5 GHz, respectively. In these figures, good omnidirectional radiation characteristics are observed.

IV. CONCLUSION

An optimal microstrip-fed monopole antenna with two F-shaped slot radiators is successfully proposed, simulated, and fabricated for WLAN/WiMAX operation. Experiments are carried out to validate the design concept and method, showing good agreement between simulations and measurements. The proposed antenna features compact size, good triband operating bandwidth, and stable radiation patterns indicating that it can be a good candidate for WLAN/WiMAX applications.

REFERENCES

- [1] W. Hu, Y.-Z. Yin, P. Fei, and X. Yang, "Compact triband square-slot antenna with symmetrical L-strips for WLAN/WiMAX applications," *IEEE Antennas Wireless Propag. Lett.*, vol. 10, no. pp. 462–465, May 2011.
- [2] L. Dang, Z. Y. Lei, Y. J. Xie, G. L. Ning, and J. Fan, "A compact microstrip slot triple-band antenna for WLAN/WiMAX applications," *IEEE Antennas Wireless Propag. Lett.*, vol. 9, pp. 1178–1181, Dec. 2010.
- [3] C.-M. Wu, C.-N. Chiu, and C.-K. Hsu, "A new non-uniform meandered and fork-type grounded antenna for triple-band WLAN applications," *IEEE Antennas Wireless Propag. Lett.*, vol. 5, no. 1, pp. 346–349, Dec. 2006.
- [4] L. Peng, C.-L. Ruan, and X.-H. Wu, "Design and operation of dual/tripleband asymmetric M-shaped microstrip patch antennas," *IEEE Trans. Antennas Propag.*, vol. 9, pp. 1069–1072, Dec. 2010.
- [5] Christo Ananth, S. Esakki Rajavel, S. Allwin Devaraj, M. Suresh Chinnathampy, "RF and Microwave Engineering (Microwave Engineering).", ACES Publishers, Tirunelveli, India, ISBN: 978-81-910-747-5-8, Volume 1, June 2014, pp:1-300.
- [6] H. Zhai, Z. Ma, Y. Han, and C. Liang, "A compact printed antenna for triple-band WLAN/WiMAX applications," *IEEE Antennas Wireless Propag. Lett.*, vol. 12, pp. 65–69, Jan. 2013.
- [7] R. Karimian, H. Oraizi, S. Fakhte, and M. Farahani, "Novel F-shaped quad-band printed slot antenna for WLAN and WiMAX MIMO systems," *IEEE Antennas Wireless Propag. Lett.*, vol. 12, pp. 405–408, Mar. 2013.
- [8] H. Chen, X. Yang, Y. Z. Yin, S. T. Fan, and J. J. Wu, "Triband planar monopole antenna with compact radiator for WLAN/WiMAX applications," *IEEE Antennas Wireless Propag. Lett.*, vol. 12, pp. 1440–1443, Oct. 2013.
- [9] X. Li, X.-W. Shi, W. Hu, P. Fei, and J.-F. Yu, "Compact triband ACS-fed monopole antenna employing open-ended slots for wireless communication," *IEEE Trans. Antennas Propag.*, vol. 12, pp. 388–391, Mar. 2013.
- [10] H. Huang, Y. Liu, S. Zhang, and S. Gong, "Multiband metamaterial loaded Monopole antenna for WLAN/WiMAX applications," *IEEE Antennas Wireless Propag. Lett.*, vol. 14, pp. 662–665, Feb. 2015.
- [11] C. Zhou, G. Wang, J. Liang, Y. Wang, and B. Zong, "Broadband antenna employing simplified MTLs for WLAN/WiMAX applications," *IEEE Antennas Wireless Propag. Lett.*, vol. 14, pp. 595–598, Apr. 2014.
- [12] S. Joshi, A. K. Gautam, and R. Upadhyay, "Frequency agile triple band microstrip antenna for WLAN/WiMAX application," *Int. J. Future Comput. Commun.*, vol. 3, pp. 258–261, 2014.
- [13] P. Liu, Y. Zou, B. Xie, X. Liu, and B. Sun, "Compact CPW-fed triband printed antenna with meandering split-ring slot for WLAN/WiMAX applications," *IEEE Antennas Wireless Propag. Lett.*, vol. 11, pp. 1242–1245, Nov. 2012.
- [14] C.-M. Peng, I.-F. Chen, and J.-W. Yeh, "Printed broadband asymmetric dual-loop antenna for WLAN/WiMAX applications," *IEEE Antennas Wireless Propag. Lett.*, vol. 12, pp. 898–901, Jul. 2013.
- [15] C. A. Balanis, *Antenna Theory Analysis and Design*, 3rd ed. Hoboken, NJ, USA: Wiley, 2005.